CellPress
REVIEWS

Review

# Responsive and Foldable Soft Materials

Jiaqi Liu,[1] Yuchong Gao,[1] Young-Joo Lee,[1,2] and Shu Yang[1,*]

**Stimulus-responsive soft materials that can enable folding of a 2D sheet into a 3D object have potential significant applications, including wearable electronics, biomimetic machines, soft robotics, drug delivery, biomedical devices, and responsive buildings. The responses can be tuned by the materials chemistry, composition, and type of external stimulus; the direction and magnitude of the deformation can be varied by geometric design and incorporation of nonresponsive materials and nanofillers. In this review, we overview different types of responsive materials (e.g., responsive hydrogels, shape memory polymers, liquid crystal elastomers, and polymer composites) and some of the basic folding mechanisms. We highlight the required material properties, fabrication techniques, and structural designs for desirable folding structures.**

## Highlights

Responsive soft materials can be deformed and folded from 2D to 3D in response to external stimuli, including pH, temperature, light, and electric and magnetic fields.

Hydrogels, shape memory polymers, liquid crystal elastomers, and polymer composites with active components are main categories of responsive soft materials. Diverse folding structures can be realized through rational design of geometries and choice of materials.

Each type of responsive soft material has its own intrinsic characteristics, enabling fine-tuning of actuation and folding behaviors, and they can be combined together to generate orthogonal responses to external stimuli. The aqueous nature of hydrogels makes them highly suitable in biomedical applications. The reprogrammability of shape memory polymers is appropriate for arbitrarily reconfigurable devices. The anisotropy of liquid crystal elastomers makes it possible to create high-strength and high-speed actuators with high energy efficiency.

## Diverse Responsive Soft Materials for Folding

Materials that can bend and fold on demand and transform from 2D to 3D structures upon exposure to external stimuli are of increasing interest to create complex structures and achieve multifunctions. Compared with hard materials, such as metals and ceramics, that are nondeformable and not adaptive like bioorganisms, soft materials are prone to deformation with large volume changes in response to an external stimulus. Thus, they offer greater degrees of freedom for realizing programmable and responsive shapes and functions over multiple lengthscales. Many are also biocompatible and biodegradable.

Recently, shape changing hydrogels, shape memory polymers (SMPs), liquid crystal elastomers (LCEs), and dielectric elastomers (DEs) have been extensively studied for potential applications, including soft robotics, biomimetic machines, tissue engineering, smart packaging, and deployable aerospace devices (see examples in Figure 1, Key Figure). Hydrogels are crosslinked polymeric networks that can undergo large volume changes when immersed in an aqueous phase [1]. SMPs can be processed to create an 'infinite' number of temporary shapes and recover back to the original shape upon heating above the phase-transition temperature [2]. The intrinsic anisotropy and reversible deformation in LCEs are reversible two-way SMPs that can be preprogrammed to achieve complex shape transformation [3]. The simple working principles, low power requirement, and fast response of DEs through capacitive actuation make them attractive for application as artificial muscles and soft robotics [4]. By inclusion of active nanofillers, such as carbon nanotubes (CNTs), silver nanowires (AgNWs), and liquid metals, passive polymers can be made light responsive [5], electric responsive [6], and electric and thermal responsive [7], respectively. Silicone rubber with embedded microchannels can be actuated pneumatically to change shapes [8]. In Table 1, we list representative responsive soft materials. Given many excellent reviews in literature on different types of responsive soft materials (such as [1–3]), this review focuses on the mechanism and performance of foldable soft materials, specifically highlighting the latest advances in both materials development and improvement of fabrication techniques.

## Geometric Design Considerations

The key principle in shape programming is to introduce 'inhomogeneity' in the materials to control the local actuation and, therefore, the targeted global shape. Inhomogeneity includes crosslinking gradients, stacking and patterning of multilayered materials of varying stiffness, and/or introducing holes or cuts, yielding preferential bending or twisting out-of-plane [9–11]. The simplest mechanical deformation is uniaxial bending when a beam shrinks or expands along a given direction (Figure 2A). When two materials, A and B, of differing thickness, $h_A$ and $h_B$, and plane-strain modulus, $\overline{E}_A$ and $\overline{E}_B$ [with $\overline{E}_i = E_i/(1-\nu_i^2)$, where $E_i$ and $\nu_i$ denote the Young's modulus and Poisson's ratio of the constituent material, respectively] are stacked together, the curvature induced by the mismatch in strain between the two materials can be estimated according to classical bending theory [9]

[1]Department of Materials Science and Engineering, University of Pennsylvania, 3231 Walnut Street, Philadelphia, PA 19104, USA

[2]Department of Electrical and Systems Engineering, University of Pennsylvania, 200 South 33rd Street, Philadelphia, PA 19104, USA

*Correspondence: shuyang@seas.upenn.edu

## Key Figure

### Schematic Illustrating Responsive and Foldable Soft Materials for Various Applications

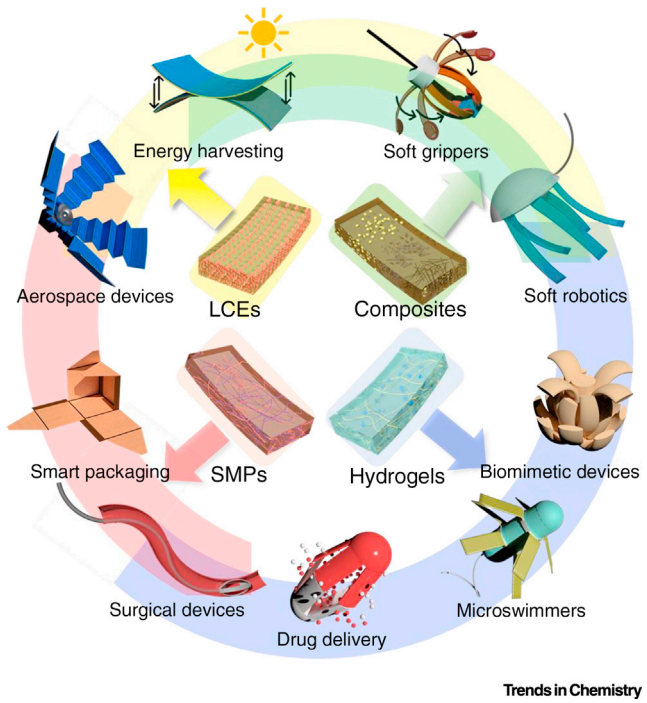


**Figure 1.** Abbreviations: LCE, liquid crystal elastomers; SMP, shape memory polymer.

$$R/h_A = (1 + 4\eta\xi + 6\eta^2\xi + 4\eta^3\xi + \eta^4\xi^2)\,/6\varepsilon_m\eta\xi(1 + \eta) \quad [1]$$

Where $R$ is the resultant curvature, $\eta = h_A/h_B$, $\xi = E_A/E_B$, and $\varepsilon_m$ is the mismatched strain. Importantly, Equation 1 assumes that all the constituent materials are linearly elastic. According to Equation 1, the magnitude of bending is determined by the strain mismatch and relative dimensions of the constituent materials. The direction of bending can be controlled by the geometric design and proper choice of the responsive materials with desired physiochemical properties.

When the direction of the tensile or compressive force exerted by responsive material deviates from the longitudinal direction of the nonresponsive layer, the bilayer can morph into a helix. Depending on where the nonresponsive layer is placed and its thickness, the final shape can be fine-tuned. For example, Jeong and colleagues patterned swellable polymer stripes on a rectangular-shaped nonresponsive polymer film, where the stripes were tilted relative to the major axis of the rectangle with periodic valleys and ridges (Figure 2B), leading to twisting in diverse directions depending on patterning geometry [12]. Inhomogeneity can also be introduced by varying the crosslinking density in polymer networks and introducing pore arrays or anisotropic molecular alignment. For example, a 2D hydrogel sheet with a radially graded crosslinking density can morph into a curved shape when swollen (Figure 2C) due to differences in volumetric expansion within the film [13].

Programming the sequence of deformation also plays an important role for achieving complex and multiple shape configurations (Figure 2D) [10,14]. For example, Liu and colleagues demonstrated sequential

## Glossary

**Auxetics**: structures or lattices that have negative Poisson's ratio; they expand in the transverse direction when stretched.
**Mechanical metamaterials**: artificial materials that exhibit mechanical properties not found in nature. These unusual properties arise not from the bulk behavior of the composing materials, but more from their structure.
**Poly(acrylic acid) (PAA)**: PAA has a pKa ~4.7, with acid groups highly protonated when pH is much lower than its pKa and with acid groups associated when pH is higher than this value. At around pKa of PAA (pH ~4.5–5.5), there is a sharp volume change attributed to the large degree of ionization of the weak acid groups.
**Poly(*N*-isopropyl acrylamide) (PNIPAAm)**: PNIPAAm has a low critical solution temperature (LCST) of ~32°C. Below the LCST, the polymer is miscible in water and the gel is swollen, and above LCST, the polymer is immiscible with water and the gel collapses out of water.

**Table 1. Representative Responsive and Foldable Soft Materials, Including Hydrogels, Shape Memory Polymers (SMPs), Liquid Crystal Elastomers (LCEs), Dielectric Elastomers (DEs), and Polymer Composites**[a]

| Materials | Chemistry | Mechanical deformation approach | Stimulus type | Potential applications | Refs |
|---|---|---|---|---|---|
| Hydrogels | PNIPAAm-based copolymer | Crosslinking gradients | Thermal | Microdevices | [31,32] |
| | PNIPAAm-based polymer | Porosity gradients | Thermal, light | Biomimetic machines | [33] |
| | PNIPAAm-based composite polymers | Chemically heterogeneous patterning | Thermal, magnetic, pH, ionic strength | Soft robotics, surgical devices, bioactuators, tissue engineering | [34–38] |
| | Cellulose/ carboxymethylcellulose, PNIPAAm with inert polymer sheets | Bilayers or trilayers | Thermal, pH, ionic strength | Biomedicine, biomimetic machines, microscopic swimmers, microrobotics, scaffolds for cell culture, microfluidics | [9,27–30] |
| | Acrylamide or PNIPAAm with cellulose nanofibrils | Anisotropic 3D structures | Thermal | Tissue engineering, soft robotics, biomedical devices | [39] |
| | PNIPAAm/MNPs, AuNPs, or RGO hydrogel composites | Bilayers, patterning | Photothermal, magnetothermal | Drug delivery, soft robotics, microfluidics, soft micromachines | [40–42] |
| SMPs | PETMP-HMDI, epoxy, PCL-thiol based network, PBMA, Tangoblack, VeroWhite | One-way shape memory | Thermal | Medical devices, consumer products, deployable aerospace devices | [43–48] |
| | PCL-based copolymer, thiol-acrylate-based double network | Triple state shape memory | Thermal | Medical devices, smart packaging | [49–52] |
| | PCL-based copolymer, thiol-acrylate-based double network, PEVA copolymers | Two-way shape memory | Thermal | Soft robotics | [45,53,55–58] |
| LCEs | Diacrylate and azobenzene based | Bilayers | Humidity, light | Electronic sensors | [70] |
| | Acrylate and azobenzene based (with chiral dopants) | Mechanical instability from twist, chiral twist, and splay configurations | Light | Autonomous soft devices, micromechanics, artificial muscles, photomechanical energy harvest, biomimetic devices | [59–62] |
| | Diacrylate with amine chain extender, oligomers from thiol-acrylate click chemistry or azobenzene | Patterning from molecular anisotropy | Thermal, light | Deployable aerospace devices, optics, medical devices, soft robotics | [72–76] |
| | Diacrylate with amine chain extender or oligomers from thiol-acrylate click chemistry | Anisotropic 3D structures | Thermal | Implantable medical devices, soft robotics, optics | [77–80] |
| | Hydroxyl and ester based | Anisotropic 3D structures or bilayers | Photothermal | Artificial muscles | [83–86] |

*(Continued on next page)*

**Table 1. *Continued***

| Materials | Chemistry | Mechanical deformation approach | Stimulus type | Potential applications | Refs |
|---|---|---|---|---|---|
| DEs | Acrylic elastomers, CNT electrodes | Multilayers with electrode patterning | Electrical | Stretchable sensors, soft robotics | [93] |
| | Acrylic elastomers with vinyl fibers, CNT electrodes | Patterning with bilayers | Electrical | Soft robotic grippers | [94] |
| | Acrylic elastomers, CNT electrodes | Multilayers with spatially varying electric fields | Electrical | Reconfigurable shape changes | [95] |
| Composites | PDMS with ethanol | Liquid–vapor transition with bilayers | Electrothermal | Soft robotics | [90] |
| | Silver nanowires with polyvinyl chloride | Joule heating with bilayers | Electrothermal | Soft robotics | [6] |
| | Shrinky dink with inks | Chemically heterogeneous patterning | Light | Smart packaging, reconfigurable actuators | [10] |
| | PI with CNTs and wax | Bilayers | Photothermal | Solar energy harvest and robotic arms | [5] |
| | Liquid metal with PDMS or Ecoflex | External mechanical instability, patterning from molecular anisotropy | Photothermal, electrothermal, mechanical | Soft robotics, reconfigurable electronics, self-healing | [7,92,96,97] |
| | Ecoflex (silicone) | Pneumatic | Pneumatic | Soft robotics, surgical devices | [8] |

[a]Abbreviations: AuNPs, gold nanoparticles; MNPs, magnetic nanoparticles; PBMA, poly(benzyl methacrylate); PCL, poly(ε-caprolactone); PDMS, polydimethylsiloxane; PETMP-HMDI, pentaerythritol tetra(3-mercaptopropionate)-hexamethylene diisocyanate; PEVA, poly[ethylene-co-(vinyl acetate)]; PI, polyimide; PNIPAAm, poly(*N*-isopropyl acrylamide); RGO, reduced graphene oxide.

self-folding of a cube when heating a 2D pre-cut, pre-stretched polystyrene sheet [10]. The hinges with diverse colors can be sequentially folded depending on the wavelength of the exposed light. Additionally, Rafsanjani and colleagues [15] designed a soft crawler with a tessellated thin shell that shrank and stretched in a longitudinal direction, twice as fast as that with a homogeneous ligament design.

Geometry is scale-invariant and material-independent. Recently, **mechanical metamaterials** (see Glossary) have been fabricated to exhibit unprecedented mechanical properties through rational design of geometry (e.g., aspect ratio of the unit size, shape, symmetry, and arrangement) instead of chemical composition [16]. One of the well-known examples is **auxetics**, which has a negative Poisson's ratio, such that the material expands in the transverse direction when pulled. Auxetic structures often consist of bars or rotating units that are connected to hinges [17]. When the hinges are bent or rotated, the entire auxetic structure expands. The behavior of typical 2D auxetics is shown in Figure 2E. In an isotropic material, the shear modulus, $G$, is determined by $G = E/(1 + \nu)$. For an auxetic material, $G$ can be strengthened for applications such as buildings or machinery, or utilized to increase plane-strain fracture toughness [18] and minimize deformation against indentation. The ability to expand upon stretching offers an opportunity to wrap a non-zero Gaussian surface without buckling [19], which is important for realizing flexible and wearable electronic devices.

A 2D sheet can be folded into 3D structures via origami (folding) or kirigami (cutting and folding). In the case of origami, folding at the crease regions allows for large volumetric changes with shape morphing. A well-known example is the Miura-ori fold (Figure 2F) [20], which has a negative Poisson's ratio more negative than –1. Recent studies of origami have focused on design rules and unraveling kinematic phenomena for various engineering applications [20–22]. For example, Chen and colleagues

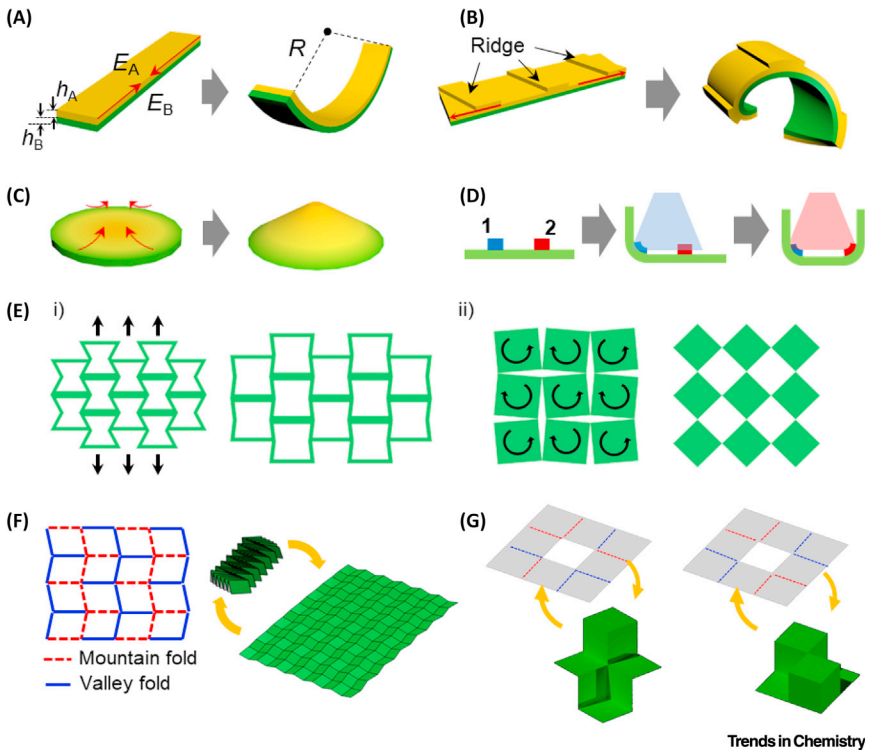


**Figure 2. Design Principles to Drive Shape Transformation.**
(A) A double-layer structure of responsive/nonresponsive film and its bending. (B) Twisting of a bilayer structure with a topologically striped pattern from the responsive material aligned deviated from the longitudinal direction of the nonresponsive substrate. (C) A responsive material with a radial crosslinking gradient can morph into non-zero Gaussian curvature. (D) Sequential folding by selective actuation. Blue and red trapezoids represent light of different wavelengths. (E) Tensile behaviors of auxetic lattices: (i) re-entrant auxetic structure, and (ii) a cut film. (F) Crease pattern and the folding/unfolding shape of a Miura origami structure. (G) Construction and configuration of a kirigami square unit, which can pop-up or pop-down.

established a comprehensive kinematic model for rigid origami panels with finite thickness [20]. Simply by changing the crease angles of a single unit Miura-fold, Liu and colleagues revealed the topological principles of origami-inspired mechanical metamaterials [21], where the kinematics was changed dramatically from being floppy and deformable to mechanically rigid and bistable.

Cutting allows for stretchability and shape morphing with different Gaussian curvatures. The rotation of the local hinges enables expandability in 2D, where the elastic properties of the material can be controlled by the design of cuts [23,24]. Through 'fractal cutting' (i.e., self-similar hierarchy) of lines, Cho and colleagues demonstrated an ~800% areal change, such that a rigid 2D sheet can conformably wrap around a baseball without wrinkles and creases [23]. By fine-tuning the placement of cuts and the angles of the adjacent rotating units, the 2D sheet of different elasticity in different regions can be preprogrammed. Besides line cuts, an array of circular holes, squares, and hexagons (or their combination) can be cut to program the shape transformation from 2D to 3D (Figure 2G) [25]. Degeneracy can be generated when transforming from one state to another when popping one unit from up-to-down or down-to-up in an array of cuts. This new found degree of freedom allows one to generate arbitrary shapes with different heights [26].

## Responsive Hydrogels

Hydrogels can undergo reversible swelling and shrinkage in response to external stimulus such as pH, temperature, and ionic strength [1]. The swelling ratio and equilibrium state of the hydrogel pattern

results from a balance of the swelling pressure and the elasticity of the polymer network that can be tailored through chemistry, composition, and the crosslinking density of the network. Thermo-responsive hydrogels such as **poly(*N*-isopropyl acrylamide) (PNIPAAm)** (Figure 3A) can undergo large volume change near the low critical solution temperature (LCST), whereas **poly(acrylic acid) (PAA)** swells when pH is greater than 5. Hydrogels are typically isotropic, that is, the shrinking and swelling is homogeneous in all directions, yet for bending and folding, it requires inhomogeneous deformation.

Forming bilayer or trilayer structures is a common strategy to introduce inhomogeneity for directed bending in hydrogel films [9,27–30]. For example, Duan and colleagues [27] fabricated a bilayer cellulose/carboxymethylcellulose sheet with opposite charge. Due to swelling ratio differences between the two layers in salt or acid solutions, a roller, a gripper, an 'S' shape, and a helical twist was formed. Xiao and colleagues [28] fabricated a gripper with eight arms made with bilayer hydrogel films of different swelling ratios in salt solutions. By introducing holes into a bilayer sheet made of PNIPAAm and a nonresponsive polymer, poly(methyl methacrylate) (PMMA), Stoychev and colleagues [29] controlled both the shape and speed of folding by varying hole position, shape, and size (Figure 3B).

Gradient soft actuators have also be realized by introducing crosslinking gradients [31,32] or porosity gradients [33]. Kim and colleagues [31] fabricated highly crosslinked dot patterns on a hydrogel matrix consisting of photosensitive benzophenone acrylamide (BPAm) and PNIPAAm via halftone lithography. By partially crosslinking the matrix, followed by a second exposure through the photomask with dotted arrays, the dotted regions possessed higher crosslinking density. After programming geometry of the dot arrays, surfaces of different Gaussian curvatures (e.g., spherical caps, saddles, and cones) and zero mean curvature were realized upon heating above the LCST of PNIPAAm (Figure 3C). Zhang and Ionov [32] synthesized hydrogel films containing the coumarin groups, where coumarin can be crosslinked in stripes at 365 nm but decoupled when irradiated to 254 nm light. The patterned film can self-fold above LCST. Luo and colleagues [33] used a hydrothermal process to create gradient porosity along the film thickness from PNIPAAm copolymers with pendant hydroxyl groups (PNIPAAM-OH). Multiple actuations, including bending, curving, twisting, and octopus-like swimming caused by thermally induced residual stress were realized.

Patterning can also be applied to create chemical heterogeneity (e.g., introducing polymers with differing stiffnesses) [34–38]. Breger and colleagues [34] combined stiff polypropylene fumarate (PPF) with soft poly(NIPAAm-*co*-AA) to program inhomogeneity in plane and created a thermally swellable self-folding microgripper. Ma and colleagues [35] selectively patterned poly(methylacrylic acid) (PMAA) onto the reduced graphene oxide (RGO)-PNIPAAm hydrogel sheet with different stiffnesses to realize different 3D shapes by varying light, pH, heat, and ionic strength. Stripes of PNIPAAm on interpenetrating network (IPN) of PNIPAAm/poly(2-acrylamido-2-propane sulfonic acid) (PAMPS) were fabricated, where the PNIPAAm stripes underwent de-swelling in high ionic strength condition while the IPN remained in the swollen state, leading to shape transformations into a short roll, a long roll, a toroid, and a helical twist, depending on pattern designs (Figure 3D) [36]. Na and colleagues [9] reported a self-foldable origami film by sandwiching the PNIPAAm layer between two patterned glassy polymer sheets made of poly(p-methylstyrene) (PpMS), consisting of open stripes with precisely controlled widths, angles, and positions such that the swelling-induced stress in the PNIPAAm layer could trigger the bending of hinges in PpMS layers, forming a bird (Figure 3E).

Heterogeneity can also be introduced in 3D printer inks. Gladman and colleagues [39] fabricated 3D structures with encoded anisotropy by formulating inks from poly(*N*,*N*-dimethyl acrylamide) or PNIPAAm mixed with cellulose nanofibrils. Upon heating, the filaments shrank preferentially in the perpendicular direction, resulting in various folding architectures that mimicked plant motion (Figure 3F). Additionally, hydrogel inks can be magnetic-responsive when mixing with magnetic nanoparticles [40] (see flagellum-like micromachine in Figure 3G) and light-responsive via the photothermal effect of RGOs and gold nanoparticles [41,42].

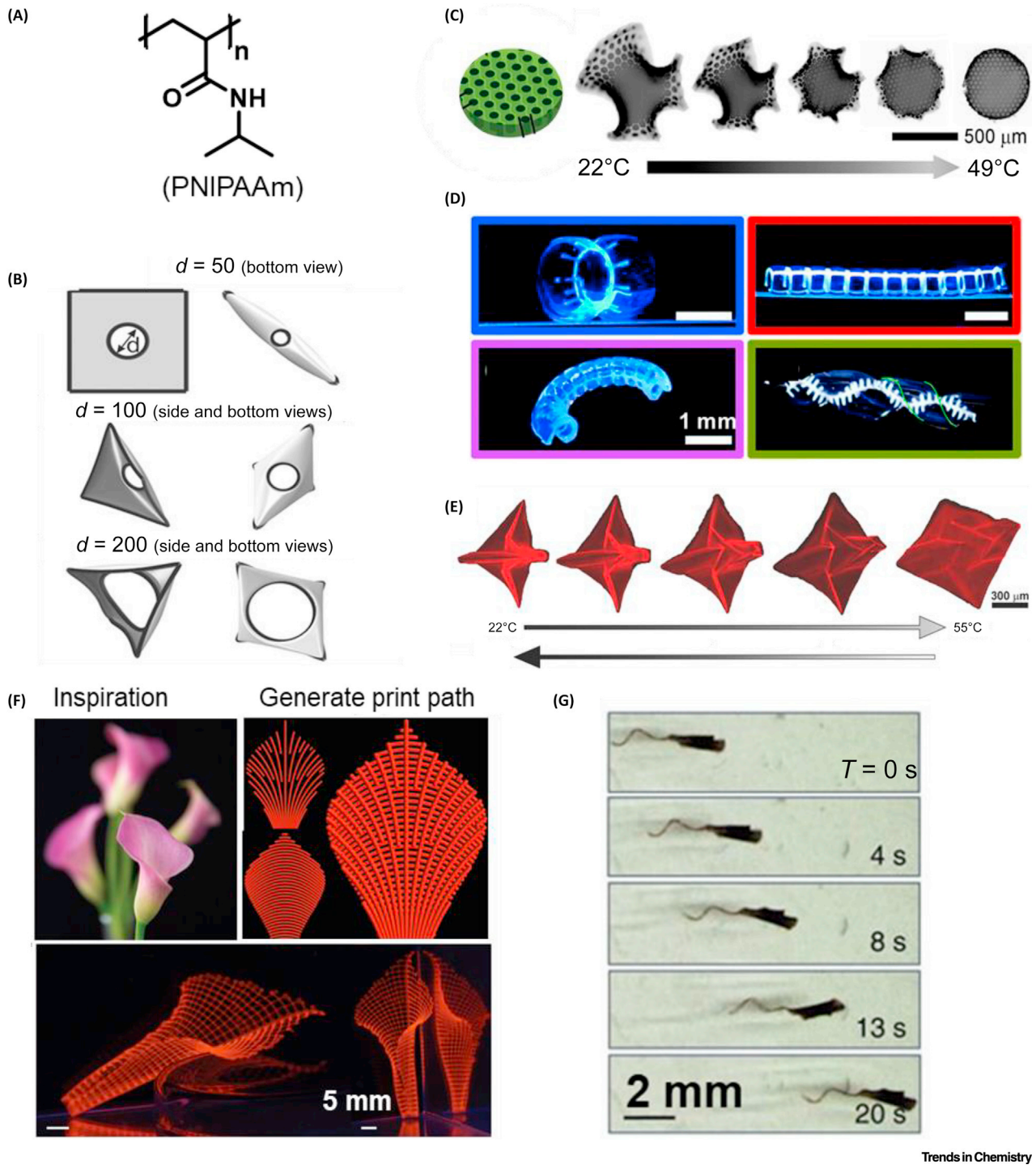


**Figure 3. Responsive Hydrogels as Foldable Soft Materials.**

(A) Chemical structure of poly(*N*-isopropyl acrylamide) (PNIPAAm). (B) Schematic and modelling of a bilayer film with different hole sizes. Adapted, with permission, from [29]. (C) Schematic illustration of the PNIPAAm hydrogel with crosslinking gradients and de-swelling of a hybrid Enneper's surface with increase in temperature. Adapted, with permission, from [31]. (D) Shape transformations of a hydrogel with striped patterns demonstrating a short roll, a long roll, a toroid, and a helical twist. Adapted, with permission, from [36]. (E) Reversible folding and unfolding of a thermally responsive origami bird. Adapted, with permission, from [9]. (F) 4D-printed thermo-responsive hydrogels mimicking calla lily. Adapted, with permission, from [39]. (G) Movement of a flagellum-like micromachine driven by magnetic fields. Adapted, with permission, from [40].

## SMPs

Control of water diffusion in and out of the hydrogel network is essential, which may not be desirable for applications that require a dry environment (e.g., dry adhesion, packaging, locomotion on land) and/or at extreme working conditions (e.g., freezing temperatures or in a desert environment). SMPs can memorize temporary shapes and recover to their permanent shape upon exposure to an external stimulus, such as heat, light, electric field, or solvent. The 'permanent' shape of SMPs is usually maintained by chemical or physical crosslinking (e.g., covalent bonding or chain entanglement). Above a thermal phase transition temperature [e.g., glass transition temperature ($T_g$) or melting temperature ($T_m$); see examples in Figure 4A, $T_g$ based epoxy and $T_m$ based poly(ε-caprolactone) (PCL)], the polymers are softened with a two-to-three order of magnitude decrease of the elastic moduli (from a few GPa to 10's MPa). Thus, they can be deformed to a 'temporary' shape that can be fixed upon cooling (Figure 4B). The entropy stored in the deformed state can be later released on demand in the shape recovery process. Compared with hydrogels, deformation of SMPs can be precisely controlled via the mechanical loading (both homogeneously and inhomogeneously). Typically, the temporary shape of SMPs is not memorized; the thermomechanical information is erased after each cycle, making them reprogrammable depending on the applied external force (see review [2]).

SMPs can be categorized as one-way, multistate, or two-way (Figure 4B–D). Conventional one-way SMPs programmed by thermomechanical cycles can have extremely complicated temporary shapes, such as an origami airplane or swan, and the programming temperature can be $T_g$ such as for pentaerythritol tetra(3-mercaptopropionate) (PETMP)-hexamethylene diisocyanate (HMDI) [43] and epoxy [44], or $T_m$ for a PCL-based network [45]. When combined with additive manufacturing techniques, the 3D SMP films can fold in a 4D fashion [46]. By mixing two of the standard 3D printing model materials, Tangoblack (a photopolymerizable thermoplastic elastomer) and VeroWhite (a more rigid, acrylic-based photopolymer) at different compositions, $T_g$ of the printed SMP can be fine-tuned to achieve sequential folding [47]. The well-controlled printing parameters combined with the inhomogeneity in the laminated structure resulted in blooming of an SMP chrysanthemum-like flower upon heating above the transition temperature (Figure 4E) [48].

By fine-tuning the chemical composition or molecular architecture, SMPs can be made to have multiple or very broad phase-transition temperatures (Figure 4C). For example, a double network of trimethylolpropane tris(3-mercaptopropionate) (TMPTMP)-trimethylolpropane triacrylate (TMPTA) and pentaerythritol tetrakis(3-mercaptoacetate) (PETMA)-divinyl sulfone (DVS) with two narrow $T_g$s [49]; star-shaped polyurethane (PU)-PCL with a broad $T_m$ [50]; poly(ethylene glycol)diol (PEG) and *N*,*N*,*N*′,*N*′-tetrakis(2-hydroxypropyl)ethylenediamine (HPED)-based PU network with a broad $T_g$ [51]; and a PCL-polyethylene glycol (PEG) double network with two distinct $T_m$s [52], all exhibited multistate shape memory effect.

When a layer of inhomogeneity or anisotropy is introduced on top of the multistate SMP, a two-way SMP can be reversibly actuated between a partially recovered state and the temporary state (Figure 4D). When anisotropy is introduced (e.g., by mechanical stretching of the film) followed by UV curing, it becomes the geometry determining domain (Figure 4F), while the rest of the network is the actuation domain. Upon cooling, crystallization in the actuation domains is guided, oriented, and coupled with the macroscopic deformation direction; upon heating, partial melting of crystallites leads to reversible actuation. The two domains can either be chemically distinct, for example, PCL as actuation domain and the stretched poly(ω-pentadecalactone) (PPD) as the geometry determining domain [53], or chemically identical, for example, partially melted poly[ethylene-*co*-(vinyl acetate)] (cPEVA) [54], where the weight ratio of the two domains can be fine-tuned to program the actuation temperature. Reprogrammability can also be achieved through exchanges of the dynamic covalent bonds in the network (e.g., via transesterification and transcarbamoylation), triggered by temperature in combination with a catalyst [55,56]. As the network undergoes macroscopic stress relaxation and plasticization, a new permanent shape is formed, which can be deformed into a new set of temporary shapes [45,55,57,58]. As shown in Figure 4G, a flat sheet made from PCL-PU-based two-way SMP can undergo bond exchange and be folded into a 3D crane. When the active region of the

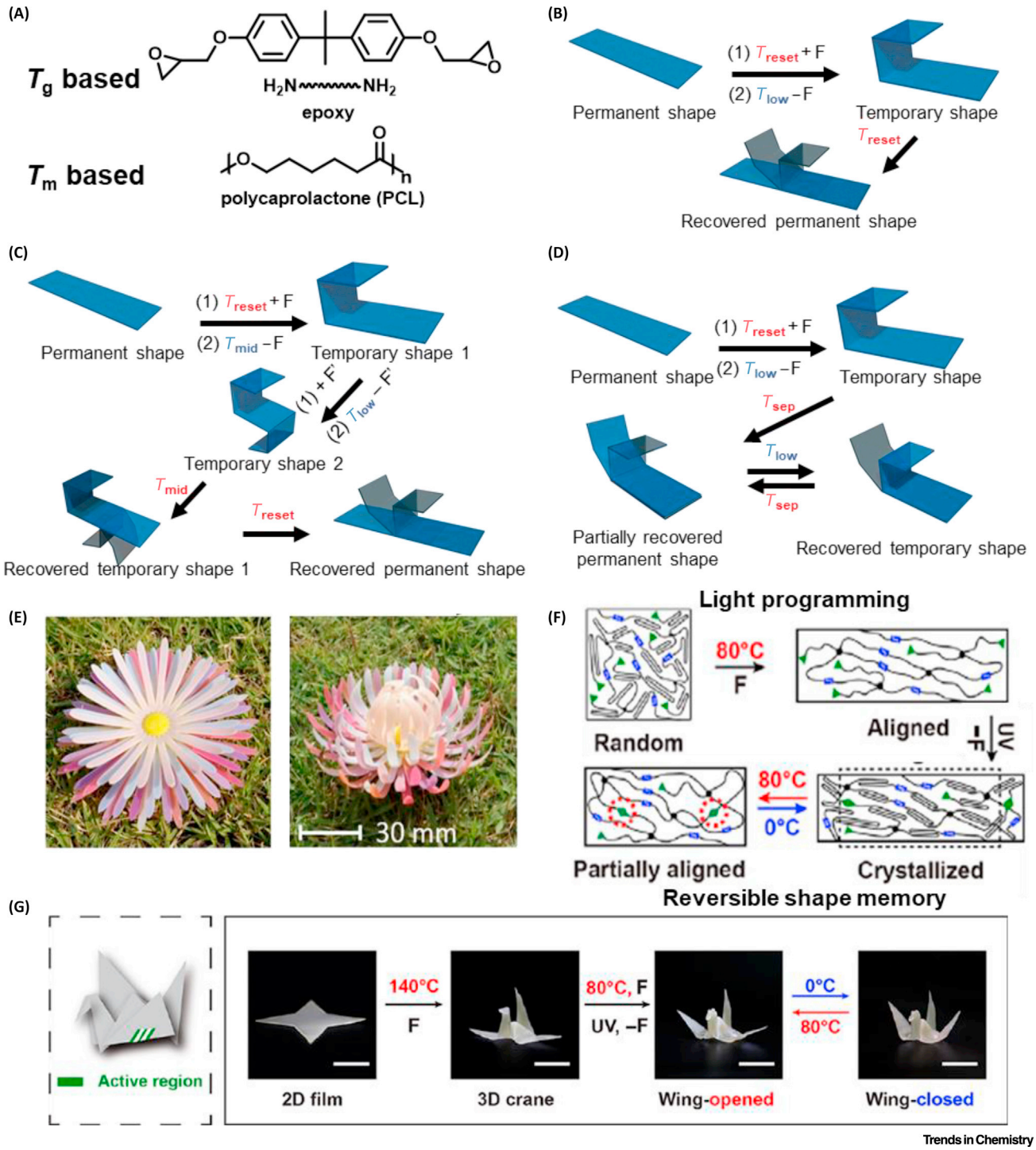


**Figure 4. Shape Memory Polymers (SMPs) as Foldable Soft Materials.**

(A) Chemical structures of typical materials for fabricating SMPs. (B) Schematic illustration of the one-way SMP working mechanism. At an elevated temperature, $T_{reset}$, the sample deforms under an applied external force (F) to a designed shape and increases the system entropy. A temporary shape is fixed when cooling down to $T_{low}$. Upon reheating above $T_{reset}$, the shape recovers. (C) Schematic illustration of the multistate SMP working mechanism. Multistate SMPs memorize multiple temporary shapes at different temperatures, $T_{mid}$ is a temperature between the two transition

*(Figure legend continued at the bottom of the next page.)*

wing underwent photo-induced dimerization, subsequent heating could recover the deformed wing, yielding flipping [57].

## LCEs

LCEs are polymer networks consisting of intrinsically anisotropic liquid crystalline (LC) molecules. They can be synthesized through radical polymerization from diacrylate-based reactive mesogen monomers (e.g., RM82) with an amine chain extender and RM82-dithiol oligomers via thiol-acrylate click chemistry (Figure 5A). LCEs undergo spontaneous and monolithic shape change driven by reorientation of the local director field of the LC mesogens when heated above the nematic (N)–isotropic (I) phase-transition temperature ($T_{NI}$) (i.e., the network contracts along the local director and expands in the perpendicular direction) and the polymer chains adopt isotropic, spherical conformations. Upon cooling, the polymer chains return to the elongated and aligned state and LCEs recover to their original shapes (Figure 5B) [3]. The phase transition can also be triggered by light [59–62], and reorientation of LC molecules can be induced by an electric field [63,64] or a magnetic field [65]. The deformation of LCE networks is highly dependent on the molecular alignment of LC molecules within the structures, allowing us to induce anisotropy in mechanical deformation, which could further amplify the deformation in-plane and induce directional shape transformation. Compared with isotropic networks such as hydrogels and conventional SMPs, LCEs are characterized with high mechanical strength and fast response (~100 ms) [66], while exhibiting large anisotropic local deformations (up to 500% strain [67]).

To control the mechanical responses (both the magnitude and direction of the local strain), it is important to align LC molecules in local domains within the network film. If the LC alignment is uniform throughout the film (i.e., monodomain), shrinking occurs along the alignment direction of the LC mesogens. Uniform LC alignment can be achieved through mechanical rubbing, stretching, shearing [68], and the use of a magnetic field [69]. For example, rubbing generates micron-sized grooves on polymer sheets that guide LC molecular orientations. Liu and colleagues [70] used a rubbed polyimide alignment layer to prepare a monodomain LCE film with acrylate and azobenzene (–N=N–) groups, exhibiting both humidity and light responsiveness (Figure 5C). The side closer to water swelled more due to formation of hydrogen bonds with carbonyl groups and ether bonds, resulting in the film bending away from the moisture.

Hybrid alignment such as splay, twist, and cholesteric configurations (Figure 5D) can be applied to introduce more complex inhomogeneity in LCEs. In a splay configuration, one side of the LCE film has uniaxial planar anchoring while the other side has homeotropic anchoring. Near $T_{NI}$, the planar anchoring side contracts more than the homeotropic anchoring side, leading to bending toward the planar anchoring side. In the example of an artificial flytrap made by Wani and colleagues [59], an approaching insect could trigger the backscattering of 488 nm light on the LCE film containing Disperse Red 1, resulting in autonomous bending to capture the insect. Twist and cholesteric configurations are usually used for helical deformations [61,62]. Iamsaard and colleagues [61] introduced chiral dopants, S-811 (left handed) and R-811 (right handed), to induce the cholesteric configurations. Depending on the handedness of helical twists and cutting angles between the ribbon and original film long axis, the final helical ribbons could exhibit winding, unwinding, and helix inversion by UV light, mimicking the cucumber tendril.

temperatures in the system. (D) Schematic illustration of the two-way SMP working mechanism. Two-way SMPs can have reversible folding/unfolding between temporary shape and partially recovered permanent shape, $T_{sep}$ is a temperature high enough to activate actuation domain, but not the geometry determining domain. (E) 3D-printed SMP flower made from Tangoblack and VeroWhite. The folding was achieved by the strain mismatch between the double layer structure and the curvature of folding was determined by the UV crosslinking gradient during 3D printing. Adapted, with permission, from [48]. (F) Working mechanism of the two-way reversible SMP. The partially aligned morphology of the geometry-determining domain was crucial for the reversible folding. Adapted, with permission, from [57]. (G) A reprogrammable polycaprolactone-polyurethane-based two-way SMP origami crane. Thermally reversible bonds, activated at 140°C, led to plastic deformation of the 2D SMP film, which can be folded into a permanent shape, 3D crane. The wing can be reprogrammed at the active region (the green area) upon UV exposure to induce reversible dimerization and flap reversibly in the heating–cooling cycles. Adapted, with permission, from [57].

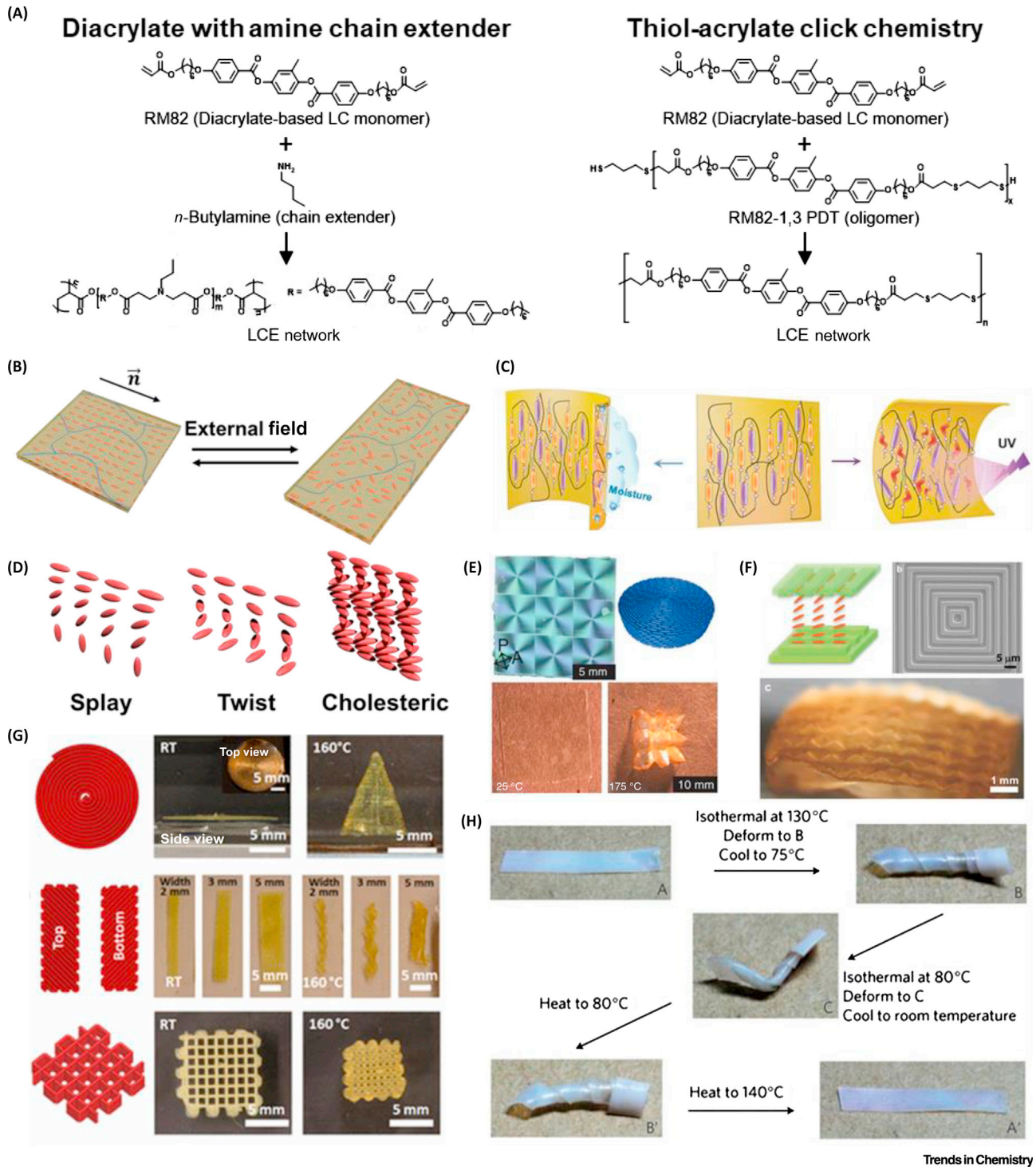


**Figure 5. Liquid Crystal Elastomers (LCEs) as Foldable Soft Materials.**

(A) Chemical structures of commonly used materials for LCE fabrication. (B) Illustration of the LCE deformation mechanism. (C) Schematic of the deformation mechanism of a humidity and light responsive LCE film. Adapted, with permission, from [70]. (D) Illustrations of cholesteric, twist, and splay configurations of liquid crystalline (LC) molecules. (E) Polarized optical microscope image of nine +1 defects (top left), a schematic showing the LC alignment around one +1

*(Figure legend continued at the bottom of the next page.)*

To realize more complex and monolithic shape change, it is essential to spatially control the LC director profile at the micron scale. Depending on boundary conditions and affinity of LCs to the surface, a jump or cusp in the continuous LC director field will lead to the formation of a singularity (so-called topological defect) in the LC phase, leading to out-of-plane deformation of LCEs into surfaces with locally controlled Gaussian curvatures, as demonstrated both theoretically [71] and experimentally [72–80]. To achieve local alignment of LC monomers with micron-scale resolution, advanced alignment methods have been introduced (see detailed review in [81]), including photoalignment [72,73], micropatterning of microchannels [74–76], and 3D printing [77–80]. In the photoalignment approach, an azobenzene-based material is used as the alignment layer, since azobenzene molecules exhibit angular-dependent absorption of incident light around 450 nm [82] and can be aligned by polarized light within the resolution of optics. Ware and colleagues [72] reported voxelated alignment in LCE films from RM82 and amine chain extender. The topological defects served as hinges and guided the folding of LCE films (Figure 5E).

Xia and colleagues [74–76] used top-down lithographic techniques to fabricate microchannels, which guided the alignment of LC molecules. In this approach, the dimension and orientation of channels can be arbitrarily controlled using photomasks with (sub)micron resolution. Figure 5F shows the thermal buckling of an LCE film with +1 and –1 defect arrays from concentric squares [74]. Xia and colleagues later reported a kirigami folding of LCE films crosslinked via thiol-acrylate click reactions [75] and inverse design to realize complex, arbitrary geometries such as a face [76].

3D printing techniques have recently been utilized to transform shapes from 3D to 3D [77–80]. Importantly, LC alignment should follow the filament long axis due to shear thinning effect [77], which can be subsequently locked by photopolymerization. The filament contracts along this axis when heated above $T_{NI}$. Oligomers from RM82 and chain extender, *n*-butylamine, were mixed as the ink to realize various folding structures, including a cone, a helical ribbon, and an in-plane contracted grid (Figure 5G) [79], a saddle shape from layered perpendicular meanders [77], and a cone array from nine '+1' defects [78]. Printed from multiple LC inks, each with a different $T_{NI}$, the obtained LCE 3D structure could demonstrate multiple and sequential folding [80].

Dynamic covalent bonds have also been applied to rewrite the alignment and reprogram LCE folding [83–86]. Pei and colleagues [83] synthesized a dynamic LCE network from decanedioic acid and biphenyl. By adding the catalyst, triazabicyclodecene, the crosslinked bonds underwent transesterification above the topology-freezing transition temperature $T_v$. In this way, mechanically induced alignment could be processed at temperature $T > T_v$ and cooled down to LC phase to fix it. Triple shape memory effect could further be realized by fixing shapes in the LC phase and below $T_g$ (Figure 5H).

Deformation of LCE films can also be controlled through localized patterning with different dyes and light irradiation at proper wavelengths [87], manipulation of dynamic and structured light on photoactive LCEs [88], and forming a bilayer structure with inert polymer film [84].

## Polymer Composites

When introducing responsive nanofillers into nonresponsive materials, the composites can be made responsive and allow for integrated sensing and actuation. CNTs and carbon nanofibers (CNFs) are known for their outstanding mechanical strength, chemical stability, and electrical and thermal conductivity. Therefore, they have been widely used as additives to create polymer composites that can be actuated by IR light [5]. The alignment of CNTs and CNFs is responsible for directing the actuation

defect (top right), and the digital images of an LCE film buckled into 3 × 3 cone arrays at 180°C (bottom). Adapted, with permission, from [72]. (F) Illustration of LC molecular alignment in microchannels (top left), scanning electron microscopy image of the fabricated microchannels (top right), and the digital image of an LCE film buckled into microcone arrays at 200°C (bottom). Adapted, with permission, from [74]. (G) Design and digital images of 3D-printed LCE structures before and after heating at 160°C. Adapted, with permission, from [79]. (H) Triple shape memory effect of a dynamic LCE network. Adapted, with permission, from [83].

directions and modes. When CNTs were perpendicularly aligned to the longitudinal direction of the polyimide substrate, tensile stress along this direction dominated, leading to bending toward to the exposed light (Figure 6Ai). When CNTs were aligned in parallel to the longitudinal direction, compressive stress along this direction dominated (Figure 6Aii). Upon exposure to light, the composite film bent in the opposite direction compared with that from the perpendicularly aligned CNTs [5]. By introducing ferromagnetic nickel coating, Stanier and colleagues reported that the incorporated short nickel-coated CNFs in polydimethylsiloxane (PDMS) can be arbitrarily aligned by the direction of external magnetic field during curing, therefore the PDMS/CNF composite can bend and twist under a homogeneous magnetic field (Figure 6B) [89].

A color changing and anisotropic actuator was fabricated by depositing percolated AgNWs on low density polyethylene (LDPE) film, followed by attachment of poly(vinyl chloride) (PVC) film on top [6]. AgNWs patterned by UV laser ablation acted as the microheater. Mismatch in the coefficient of thermal expansion between LDPE film and PVC film induced anisotropic bending along the longitudinal direction upon Joule heating. Combined with thermochromic pigment, the actuator displayed bending and color shifting simultaneously (Figure 6C). Figure 6D shows an example of a thermally driven actuator exploiting liquid–vapor transition of ethanol microbubbles in silicone [90], allowing for weightlifting approximately 1700 times of its own weight.

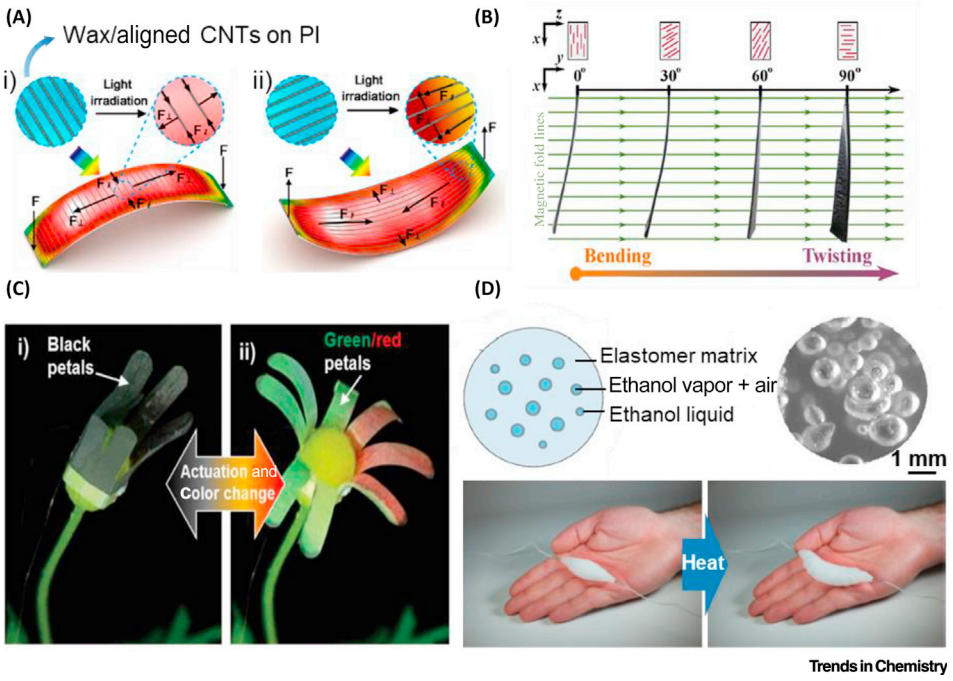


**Figure 6. Polymer Composites as Foldable Soft Materials.**
(A) Illustration of carbon nanotube (CNT)/wax composite film on the polyimide (PI) substrate with opposite bending directions, depending on CNT alignment. Two strain components, the longitudinal strain and the transverse strain, were controlled to drive bending in the opposite direction of light. Adapted, with permission, from [5]. (B) Alignment direction-dependent bending and twisting of CNT/polydimethylsiloxane (PDMS) composite film under a uniform magnetic field. Adapted, with permission, from [89]. (C) Joule heating-driven bending of poly(vinyl chloride)/ silver nanowire/low density polyethylene film. Combined with thermochromic pigment, the actuator showed bending and color shifting, simultaneously. Adapted, with permission, from [6]. (D) Schematic (left) and scanning electron microscopy image (right) of ethanol-dispersed silicone rubber composite. The composite underwent large volumetric expansion by vaporization of dispersed ethanol, which can be electrically actuated by Joule heating. Adapted, with permission, from [90].

## Concluding Remarks

We have briefly reviewed recent advances in foldable and responsive soft materials, including hydrogels, SMPs, LCEs, and polymer composites, by manipulating the inhomogeneity through the design of geometry and chemistry. Each type of material has its own unique characteristics and uses. Specifically, the aqueous nature of hydrogels makes the foldable structures suitable for biomedical applications, whereas the large volume change make hydrogels attractive for dramatic shape changes. SMPs can be deformed into many temporary shapes, which could, however, be permanently fixed through bond exchanges to start a new set of temporary shapes. LCEs can be preprogrammed to achieve complex shapes reversibly with high energy efficiency and fast switching speed. Nevertheless, many practical challenges remain (see Outstanding Questions). For example, most soft materials do not exhibit strong mechanical strength against extreme working conditions such as high pressure and low temperature (e.g., in oceanic trenches and outer space) and they suffer fatigue after repeated loading at a constant strain, a common failure mechanism in elastomers due to their viscoelastic nature [91]. Thus, the mechanical responses become less pronounced over time.

For some applications such as drug delivery, the (un)folding speed might be slow but materials have to be compatible with a fluid environment, whereas for robotic applications, stiffness, actuation speed, and load bearing capability is critical. To achieve complicated and sequential folding, geometric designs and incorporation of functional nanofillers, such as CNTs, liquid metals, and cellulose nanocrystals, will be essential to increase the 'intelligence' of the soft materials. Further, introduction of machine learning could greatly reduce the computation time and cost in designs and fabrication and provide additional functions, such as self-healing and self-repair [92].

**Outstanding Questions**

How many cycles can soft materials be actuated without losing their performance?

How many targeted shapes can the soft materials be programmed and reprogrammed?

How fast and how slow can soft materials respond to external stimuli for different applications? Can we integrate fast and slow responses in a single material?

Can we integrate different responsive soft materials into a single system to have orthogonal responses?

Can the responsiveness be achieved by low energy input while maintaining the fast response speed?

Can we use machine learning to increase the fabrication efficiency of multifunctional and sequentially foldable soft materials and/or direct their self-actuation into different shapes given environmental obstacles?

## Acknowledgments

The authors acknowledge funding from National Science Foundation (NSF) through the University of Pennsylvania Materials Research Science and Engineering Center (MRSEC) (DMR-1720530) and Army Research Offices (ARO) through the Multidisciplinary University Research Initiative (MURI) program, ARO #W911-NF-1810327 (Topic Chief, Samuel Stanton).

## References

1. Zhang, Y.S. and Khademhosseini, A. (2017) Advances in engineering hydrogels. *Science* 356, eaaf3627
2. Lendlein, A. and Gould, O.E.C. (2019) Reprogrammable recovery and actuation behaviour of shape-memory polymers. *Nat. Rev. Mater.* 4, 116
3. White, T.J. and Broer, D.J. (2015) Programmable and adaptive mechanics with liquid crystal polymer networks and elastomers. *Nat. Mater.* 14, 1087–1098
4. Brochu, P. and Pei, Q. (2010) Advances in dielectric elastomers for actuators and artificial muscles. *Macromol. Rapid Commun.* 31, 10–36
5. Deng, J. *et al.* (2016) Tunable photothermal actuators based on a pre-programmed aligned nanostructure. *J. Am. Chem. Soc.* 138, 225–230
6. Kim, H. *et al.* (2018) Biomimetic color changing anisotropic soft actuators with integrated metal nanowire percolation network transparent heaters for soft robotics. *Adv. Funct. Mater.* 28, 1801847
7. Ford, M.J. *et al.* (2019) A multifunctional shape-morphing elastomer with liquid metal inclusions. *Proc. Natl. Acad. Sci. U. S. A.* 116, 21438–21444
8. Moseley, P. *et al.* (2016) Modeling, design, and development of soft pneumatic actuators with finite element method. *Adv. Eng. Mater.* 18, 978–988
9. Na, J.-H. *et al.* (2015) Programming reversibly self-folding origami with micropatterned photo-crosslinkable polymer trilayers. *Adv. Mater.* 27, 79–85
10. Liu, Y. *et al.* (2017) Sequential self-folding of polymer sheets. *Sci. Adv.* 3, e1602417
11. Silverberg, J.L. *et al.* (2015) Origami structures with a critical transition to bistability arising from hidden degrees of freedom. *Nat. Mater.* 14, 389–393
12. Jeong, J. *et al.* (2017) Topography-guided buckling of swollen polymer bilayer films into three-dimensional structures. *Soft Matter* 13, 956–962
13. Sharon, E. (2012) Swell approaches for changing polymer shapes. *Science* 335, 1179–1180
14. Coulais, C. *et al.* (2018) Multi-step self-guided pathways for shape-changing metamaterials. *Nature* 561, 512–515
15. Rafsanjani, A. *et al.* (2019) Propagation of pop ups in kirigami shells. *Proc. Natl. Acad. Sci. U. S. A.* 116, 8200–8205
16. Surjadi, J.U. *et al.* (2019) Mechanical metamaterials and their engineering applications. *Adv. Eng. Mater.* 21, 1800864
17. Lim, T.-C. (2015) *Auxetic Materials and Structures*, Springer
18. Mir, M. *et al.* (2014) Review of mechanics and applications of auxetic structures. *Adv. Mater. Sci. Eng.* 2014, 1–17
19. Evans, K.E. and Alderson, A. (2000) Auxetic materials: functional materials and structures from lateral thinking! *Adv. Mater* 12, 617–628
20. Chen, Y. *et al.* (2015) Origami of thick panels. *Science* 349, 396–400
21. Liu, B. *et al.* (2018) Topological kinematics of origami metamaterials. *Nat. Phys.* 14, 811–815
22. Faber, J.A. *et al.* (2018) Bioinspired spring origami. *Science* 359, 1386–1391
23. Cho, Y. *et al.* (2014) Engineering the shape and structure of materials by fractal cut. *Proc. Natl. Acad. Sci. U. S. A.* 111, 17390–17395

24. Blees, M.K. *et al.* (2015) Graphene kirigami. *Nature* 524, 204–207
25. Yang, S. *et al.* (2016) Design of super-conformable, foldable materials via fractal cuts and lattice kirigami. *MRS Bull.* 41, 130–138
26. Sussman, D.M. *et al.* (2015) Algorithmic lattice kirigami: a route to pluripotent materials. *Proc. Natl. Acad. Sci. U. S. A.* 112, 7449–7453
27. Duan, J. *et al.* (2017) Bilayer hydrogel actuators with tight interfacial adhesion fully constructed from natural polysaccharides. *Soft Matter* 13, 345–354
28. Xiao, S. *et al.* (2017) Salt-responsive bilayer hydrogels with pseudo-double-network structure actuated by polyelectrolyte and antipolyelectrolyte effects. *ACS Appl. Mater. Interfaces* 9, 20843–20851
29. Stoychev, G. *et al.* (2016) Hole-programmed superfast multistep folding of hydrogel bilayers. *Adv. Funct. Mater.* 26, 7733–7739
30. Jeon, S.-J. and Hayward, R.C. (2017) Reconfigurable microscale frameworks from concatenated helices with controlled chirality. *Adv. Mater.* 29, 1606111
31. Kim, J. *et al.* (2012) Designing responsive buckled surfaces by halftone gel lithography. *Science* 335, 1201–1205
32. Zhang, Y. and Ionov, L. (2015) Reversibly cross-linkable thermoresponsive self-folding hydrogel films. *Langmuir* 31, 4552–4557
33. Luo, R. *et al.* (2015) Gradient porous elastic hydrogels with shape-memory property and anisotropic responses for programmable locomotion. *Adv. Funct. Mater.* 25, 7272–7279
34. Breger, J.C. *et al.* (2015) Self-folding thermo-magnetically responsive soft microgrippers. *ACS Appl. Mater. Interfaces* 7, 3398–3405
35. Ma, C. *et al.* (2016) A multiresponsive anisotropic hydrogel with macroscopic 3D complex deformations. *Adv. Funct. Mater.* 26, 8670–8676
36. Thérien-Aubin, H. *et al.* (2015) Shape transformations of soft matter governed by bi-axial stresses. *Soft Matter* 11, 4600–4605
37. Wu, Z.L. *et al.* (2013) Three-dimensional shape transformations of hydrogel sheets induced by small-scale modulation of internal stresses. *Nat. Commun.* 4, 1586
38. Morales, D. *et al.* (2016) Bending of responsive hydrogel sheets guided by field-assembled microparticle endoskeleton structures. *Small* 12, 2283–2290
39. Gladman, A.S. *et al.* (2016) Biomimetic 4D printing. *Nat. Mater.* 15, 413–418
40. Huang, H.-W. *et al.* (2016) Soft micromachines with programmable motility and morphology. *Nat. Commun.* 7, 12263
41. Kim, D. *et al.* (2016) Highly bendable bilayer-type photo-actuators comprising of reduced graphene oxide dispersed in hydrogels. *Sci. Rep.* 6, 20921
42. Hauser, A.W. *et al.* (2015) Photothermally reprogrammable buckling of nanocomposite gel sheets. *Angew. Chem. Int. Ed.* 54, 5434–5437
43. McBride, M.K. *et al.* (2018) Thermoreversible folding as a route to the unique shape-memory character in ductile polymer networks. *ACS Appl. Mater. Interfaces* 10, 22739–22745
44. Chen, C.-M. *et al.* (2013) Buckling-based strong dry adhesives via interlocking. *Adv. Funct. Mater.* 23, 3813–3823
45. Zhao, Q. *et al.* (2016) Shape memory polymer network with thermally distinct elasticity and plasticity. *Sci. Adv.* 2, e1501297
46. Zhang, Y. *et al.* (2019) 4D printing of a digital shape memory polymer with tunable high performance. *ACS Appl. Mater. Interfaces* 11, 32408–32413
47. Mao, Y. *et al.* (2015) Sequential self-folding structures by 3D printed digital shape memory polymers. *Sci. Rep.* 5, 13616
48. Ding, Z. *et al.* (2017) Direct 4D printing via active composite materials. *Sci. Adv.* 3, e1602890
49. Chatani, S. *et al.* (2014) Triple shape memory materials incorporating two distinct polymer networks formed by selective thiol–Michael addition reactions. *Macromolecules* 47, 4949–4954
50. Yang, X. *et al.* (2014) Triple shape memory effect of star-shaped polyurethane. *ACS Appl. Mater. Interfaces* 6, 6545–6554
51. Zheng, N. *et al.* (2017) Catalyst-free thermoset polyurethane with permanent shape reconfigurability and highly tunable triple-shape memory performance. *ACS Macro Lett.* 6, 326–330
52. Bellin, I. *et al.* (2006) Polymeric triple-shape materials. *Proc. Natl. Acad. Sci. U. S. A.* 103, 18043–18047
53. Song, H. *et al.* (2019) Synergetic chemical and physical programming for reversible shape memory effect in a dynamic covalent network with two crystalline phases. *ACS Macro Lett.* 8, 682–686
54. Behl, M. *et al.* (2013) Temperature-memory polymer actuators. *Proc. Natl. Acad. Sci. U. S. A.* 110, 12555–12559
55. Zou, W. *et al.* (2017) Dynamic covalent polymer networks: from old chemistry to modern day innovations. *Adv. Mater.* 29, 1606100
56. Kloxin, C.J. and Bowman, C.N. (2013) Covalent adaptable networks: smart, reconfigurable and responsive network systems. *Chem. Soc. Rev.* 42, 7161–7173
57. Jin, B. *et al.* (2018) Programming a crystalline shape memory polymer network with thermo- and photo-reversible bonds toward a single-component soft robot. *Sci. Adv.* 4, eaao3865
58. Zheng, N. *et al.* (2016) Thermoset shape-memory polyurethane with intrinsic plasticity enabled by transcarbamoylation. *Angew. Chem. Int. Ed.* 55, 11421–11425
59. Wani, O.M. *et al.* (2017) A light-driven artificial flytrap. *Nat. Commun.* 8, 15546
60. Gelebart, A.H. *et al.* (2017) Making waves in a photoactive polymer film. *Nature* 546, 632–636
61. Iamsaard, S. *et al.* (2014) Conversion of light into macroscopic helical motion. *Nat. Chem.* 6, 229–235
62. Wang, M. *et al.* (2016) A plant tendril mimic soft actuator with phototunable bending and chiral twisting motion modes. *Nat. Commun.* 7, 13981
63. Lehmann, W. *et al.* (2001) Giant lateral electrostriction in ferroelectric liquid-crystalline elastomers. *Nature* 410, 447
64. Davidson, Z.S. *et al.* (2019) Monolithic shape-programmable dielectric liquid crystal elastomer actuators. *Sci. Adv.* 5, eaay0855
65. Kaiser, A. *et al.* (2009) Magnetoactive liquid crystal elastomer nanocomposites. *J. Mater. Chem.* 19, 538–543
66. Camacho-Lopez, M. *et al.* (2004) Fast liquid-crystal elastomer swims into the dark. *Nat. Mater.* 3, 307
67. Ahir, S.V. *et al.* (2006) Self-assembled shape-memory fibers of triblock liquid-crystal polymers. *Adv. Funct. Mater.* 16, 556–560
68. Küpfer, J. and Finkelmann, H. (1991) Nematic liquid single crystal elastomers. *Makromol. Chem. Rapid Commun.* 12, 717–726
69. Yang, H. *et al.* (2009) Micron-sized main-chain liquid crystalline elastomer actuators with ultralarge amplitude contractions. *J. Am. Chem. Soc.* 131, 15000–15004
70. Liu, Y. *et al.* (2017) Humidity- and photo-induced mechanical actuation of cross-linked liquid crystal polymers. *Adv. Mater.* 29, 1604792
71. Modes, C.D. and Warner, M. (2011) Blueprinting nematic glass: systematically constructing and combining active points of curvature for emergent morphology. *Phys. Rev. E Stat. Nonlin. Soft Matter Phys.* 84, 021711

72. Ware, T.H. *et al.* (2015) Voxelated liquid crystal elastomers. *Science* 347, 982–984
73. Guin, T. *et al.* (2018) Layered liquid crystal elastomer actuators. *Nat. Commun.* 9, 2531
74. Xia, Y. *et al.* (2016) Guided folding of nematic liquid crystal elastomer sheets into 3D via patterned 1D microchannels. *Adv. Mater.* 28, 9637–9643
75. Xia, Y. *et al.* (2018) Instant locking of molecular ordering in liquid crystal elastomers by oxygen-mediated thiol–acrylate click reactions. *Angew. Chem. Int. Ed.* 57, 5665–5668
76. Aharoni, H. *et al.* (2018) Universal inverse design of surfaces with thin nematic elastomer sheets. *Proc. Natl. Acad. Sci. U. S. A.* 115, 7206–7211
77. Kotikian, A. *et al.* (2018) 3D printing of liquid crystal elastomeric actuators with spatially programed nematic order. *Adv. Mater.* 30, 1706164
78. López-Valdeolivas, M. *et al.* (2018) 4D printed actuators with soft-robotic functions. *Macromol. Rapid Commun.* 39, 1700710
79. Ambulo, C.P. *et al.* (2017) Four-dimensional printing of liquid crystal elastomers. *ACS Appl. Mater. Interfaces* 9, 37332–37339
80. Saed, M.O. *et al.* (2019) Molecularly-engineered, 4D-printed liquid crystal elastomer actuators. *Adv. Funct. Mater.* 29, 1806412
81. Xia, Y. *et al.* (2019) Tailoring surface patterns to direct the assembly of liquid crystalline materials. *Liq. Cryst. Rev.* 7, 30–59
82. Weigert, F. (1921) Über einen neuen effekt der strahlung. *Sci. Nat.* 9, 583–588
83. Pei, Z. *et al.* (2014) Mouldable liquid-crystalline elastomer actuators with exchangeable covalent bonds. *Nat. Mater.* 13, 36–41
84. Lu, X. *et al.* (2018) Liquid-crystalline dynamic networks doped with gold nanorods showing enhanced photocontrol of actuation. *Adv. Mater.* 30, 1706597
85. Yang, Y. *et al.* (2016) Making and remaking dynamic 3D structures by shining light on flat liquid crystalline vitrimer films without a mold. *J. Am. Chem. Soc.* 138, 2118–2121
86. Pei, Z. *et al.* (2016) Regional shape control of strategically assembled multishape memory vitrimers. *Adv. Mater.* 28, 156–160
87. Gelebart, A.H. *et al.* (2017) A rewritable, reprogrammable, dual light-responsive polymer actuator. *Angew. Chem. Int. Ed.* 56, 13436–13439
88. Palagi, S. *et al.* (2016) Structured light enables biomimetic swimming and versatile locomotion of photoresponsive soft microrobots. *Nat. Mater.* 15, 647–653
89. Stanier, D.C. *et al.* (2016) Fabrication and characterisation of short fibre reinforced elastomer composites for bending and twisting magnetic actuation. *Compos. Part Appl. Sci. Manuf.* 91, 168–176
90. Miriyev, A. *et al.* (2017) Soft material for soft actuators. *Nat. Commun.* 8, 596
91. Tanaka, Y. *et al.* (2000) Fracture energy of gels. *Eur. Phys. J. E* 3, 395–401
92. Markvicka, E.J. *et al.* (2018) An autonomously electrically self-healing liquid metal–elastomer composite for robust soft-matter robotics and electronics. *Nat. Mater.* 17, 618
93. Duduta, M. *et al.* (2016) Multilayer dielectric elastomers for fast, programmable actuation without prestretch. *Adv. Mater.* 28, 8058–8063
94. Shian, S. *et al.* (2015) Dielectric elastomer based "grippers" for soft robotics. *Adv. Mater.* 27, 6814–6819
95. Hajiesmaili, E. and Clarke, D.R. (2019) Reconfigurable shape-morphing dielectric elastomers using spatially varying electric fields. *Nat. Commun.* 10, 183
96. Yun, G. *et al.* (2019) Liquid metal-filled magnetorheological elastomer with positive piezoconductivity. *Nat. Commun.* 10, 1300
97. Joshipura, I.D. *et al.* (2018) Patterning and reversible actuation of liquid gallium alloys by preventing adhesion on rough surfaces. *ACS Appl. Mater. Interfaces* 10, 44686–44695